

# Laser-induced phase segregation of inorganic halide perovskite alloy nanowires for optical switch

Qihang Lv<sup>1,§</sup>, Xia Shen<sup>1,§</sup>, Xuyang Li<sup>1</sup>, Jianzhe Liu<sup>2</sup>, Zhaohui Shan<sup>1</sup>, Liantuan Xiao<sup>1</sup>, Pengfei Guo<sup>1</sup>, and Johnny C. Ho<sup>3,4</sup>


<sup>1</sup> College of Physics and Optoelectronics, Taiyuan University of Technology, Taiyuan 030024, China

<sup>2</sup> Huangshan Bright Semiconductor Co., Ltd., Huangshan 245021, China

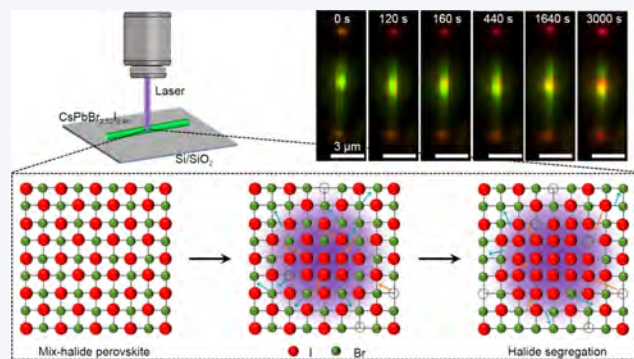
<sup>3</sup> Department of Materials Science and Engineering, City University of Hong Kong, Kowloon, Hong Kong 999077, China

<sup>4</sup> Institute for Materials Chemistry and Engineering, Kyushu University, Fukuoka 819-0395, Japan

<sup>§</sup> Qihang Lv and Xia Shen contributed equally to this work.

 Cite this article: *Nano Research*, 2025, 18, 94907119. <https://doi.org/10.26599/NR.2025.94907119>

**ABSTRACT:** Inorganic perovskite nanostructures have attracted considerable attention for their tunable band gaps and excellent optoelectronic properties. It is inevitable that phase segregation of halide perovskite usually occurs in mixed-halide perovskites under a focused laser illumination, which caused by photo-induced halide-ion segregation. Here, we reported an uniform perovskite alloy nanowires via a chemical vapor deposition (CVD) method. Microstructural characterization reveals that these perovskite nanowires have independent linear morphology with high-quality crystalline. Micro-photoluminescence (PL) spectra exhibit that these nanowire structures show a dual-wavelength emissions at 690 and 570 nm, respectively. Additionally, time-dependent PL intensity of the emission peak at 690 nm is increased by the decrease of the emission peak at 570 nm under a focused laser illumination, indicating the formation of phase segregation at the excited positions. Moreover, based on these as-grown halide perovskite CsPbBr<sub>2.52</sub>I<sub>0.48</sub> nanowires, a reasonably optical switch is designed and constructed. This optical switch may have potential applications in timed blasting system and time-delay circuit in the future.



**KEYWORDS:** perovskite alloy nanowires, phase segregation, dual-wavelength emission, optical switch, nanophotonics

## 1 Introduction

All-inorganic metal lead halide perovskites have emerged as promising semiconductor materials due to their excellent properties, such as high photoluminescence quantum yield (PLQY), long carrier diffusion length, good defect tolerance and widely tunable bandgap [1–9]. Significant research efforts have been made in the photonic and photoelectric field, including nano/micro-scale lasers [10–12], solar cells [13, 14], light-emitting devices (LEDs) [15, 16], photodetectors [17, 18] and optical switches [19, 20] et al. Moreover, metal halide perovskites appear as highly dynamic

systems, whereby the change of phase is a familiar phenomenon in halide perovskite materials, in which different phases exhibit distinctive optoelectronic properties [21, 22].

Halide perovskites exhibit diverse structure phases that giving rise to significant structural difference without composition change [3, 23, 24], which represents an ideal platform to investigate phase change processes [25]. To date, various research based on the phase transition or phase segregation of perovskites have been demonstrated [26–31]. For example, controllability of various temperature-dependent phase transition based on the individual CsPbI<sub>3</sub> nanowires was demonstrated by varying the moisture level and temperature [32]. The CsSnI<sub>3</sub> nanowire based p–n heterojunctions were constructed via a localized phase transition by heating processes [33]. The suppression of phase segregation in mixed-halide CsPbBr<sub>1.2</sub>I<sub>1.8</sub> nanocrystals was reported through a periodic heating method [34]. The occur of phase segregation in CsPbBr<sub>1.2</sub>I<sub>1.8</sub> nanocrystals as a reversible blue shift of PL peak was realized by controlling the switch of light [35]. In fact, the phase

Received: October 8, 2024; Revised: November 2, 2024

Accepted: November 7, 2024

✉ Address correspondence to Pengfei Guo, [guopengfei2010@126.com](mailto:guopengfei2010@126.com); Xia Shen, [shenxia2019@126.com](mailto:shenxia2019@126.com)

segregation of mixed-halide perovskites [23, 36–41] provides more possibilities in perovskite-based photonic devices, owing to the modification of the homogeneous energy landscape for charge carriers [39, 42]. Therefore, constructing devices reasonably based on the phase segregation in mixed-halide perovskite materials may bring new possibilities in photonics and optoelectronics devices in the future.

In this work, we report a two-step chemical vapor deposition (CVD) method to fabricate high-quality self-assembled  $\text{CsPbBr}_{2.52}\text{I}_{0.48}$  alloy nanowires. Scanning electron microscopy (SEM) and energy-dispersive X-ray (EDX) results prove that these self-assembled nanowires have uniform element distribution before and after the phase segregation. The optical characterization indicate that nanowires have dual emission with peaks at 570 and 690 nm as a consequence of halide ion segregation. The PL intensity of the emission peak at 690 nm increased gradually with the decrease of emission peak centered at 570 nm under a continuous laser illumination, which owing to the phase segregation from the mixed phase to the separated phase under a laser excitation. Moreover, optical switch based on the  $\text{CsPbBr}_{2.52}\text{I}_{0.48}$  nanowires are fabricated at room temperature. These results may provide an opportunity for multifunctional optical switching devices in the future.

## 2 Experimental

### 2.1 Materials and methods

The self-assembled perovskite  $\text{CsPbBr}_{2.52}\text{I}_{0.48}$  alloy nanowires were grown via a source-moving CVD methods, as shown in Fig. S1 in the Electronic Supplementary Material (ESM). A horizontal furnace (OTF-1200X) was used to grow the materials with a quartz tube (inner diameter 45 mm, length 180 cm). Two quartz boats equipped with  $\text{PbI}_2/\text{CsI}$  and  $\text{PbBr}_2/\text{CsBr}$  (Alfa Aesar, 99.99%, mole ratio = 1:2) and connected by quartz rods are placed in the central heating area and upstream, respectively. Several pieces of  $\text{Si}/\text{SiO}_2$  (4 mm × 10 mm) substrates were placed at the deposition area for the growth of nanostructures. Before heating, a  $\text{N}_2$  gas flow (100 sccm) was pumped into the system for 30 min to vent off the air from the cavity. Then,  $\text{N}_2$  gas flow (50 sccm) and  $\text{H}_2$  gas flow (10 sccm) were introduced into the chamber and the pressure was controlled at 5 Torr during the entire experiment. Notably, the right zone was first ramped up to 290 °C at a rate of 25 °C/min before growth, in which temperature of the substrates was located. Then, the temperature of left zone was ramped up to 420 °C at a rate of 25 °C/min. After 60 min, the temperature of the two zones was reduced to 390 and 290 °C at a rate of 10 °C/min. At the same time, the quartz boat carrying  $\text{PbBr}_2/\text{CsBr}$  is pushed into the center of the heating zone through a stepper motor. Finally, the furnace cool down naturally after 90 min. During the growth process, the alloy components are prepared by ion displacement.

### 2.2 Materials characterization

The morphologies of nanowires were investigated via SEM (Hitachi SU-8010, Japan) with energy dispersive X-ray spectroscopy (EDX) probe. The nanowire was transferred to a specific location on the substrate through three-dimensional (3D) mechanical arms with homemade fiber probes for EDX analyses of the same nanowire before and after laser irradiation. The crystal structures were determined by transmission electron microscopy (TEM, JEM-

F200). The nanowire was transferred from the primary substrate to the copper grid through 3D mechanical arms with homemade fiber probes, as shown in Fig. S2 in the ESM. Optical characterization was test by a confocal optical system. PL spectra were recorded by an Ocean Optics Spectrometer (MayaPro2000) with laser beams (375 nm,  $P = 9.7 \times 10^2 \text{ W/cm}^2$ ) focused to 1.5  $\mu\text{m}$  by a microscope (Nikon, × 100) and locally excited the nanowire.

## 3 Results and discussion

The self-assembled  $\text{CsPbBr}_{2.52}\text{I}_{0.48}$  nanowires were fabricated on a  $\text{Si}/\text{SiO}_2$  substrate using a two-step CVD method as shown in Fig. S1 in the ESM (and see the experimental section). Figures 1(a)–1(e) show low- and high-resolution SEM images of the prepared nanowires, which have a regular square shaped cross section with a wire length of 3–20  $\mu\text{m}$  and a side length of 300–700 nm (Figs. 1(c)–1(e)). Figures 1(f) and 1(g) show the two-dimensional (2D) element mapping and line scans of a typical nanowire respectively, which suggest an uniform distribution of the Cs, Pb, Br and I along the length of nanowire. The composition uniformity of nanowire is further demonstrated by the EDX mapping of cross sections (Fig. S3 in the ESM). The EDX spectra from three typical positions (as indicated in Fig. 1(f)) of a wire is shown in Fig. 1(h), which exhibit the atomic ratio of Cs, Pb, Br and I is close to 1:1:2.52:0.48. In order to further investigate the microstructures of the wires, a selected representative nanowire is transferred from a  $\text{Si}/\text{SiO}_2$  substrate to a micro-grid via a 3D platform with the homemade fiber probes under an optical microscope, as shown in Fig. S2 in the ESM. Figure 1(i) shows the low-resolution TEM image of a nanowire with the length of ~ 12  $\mu\text{m}$  and diameter of ~ 500 nm. The high-resolution TEM (HR-TEM) images taken from two typical positions (red and blue squares as indicated in Fig. 1(i)) along the axial direction of the nanowire are exhibited in Figs. 1(j) and 1(k), with a lattice spacing of ~ 0.293 nm, which corresponding to the (200) lattice spacing of the orthorhombic phase  $\text{CsPbBr}_{2.52}\text{I}_{0.48}$  [43]. The corresponding fast Fourier transform (FFT) pattern is shown in inset image of Fig. 1(j). From the combined FFT and TEM characterizations, we can conclude that self-assembled  $\text{CsPbBr}_{2.52}\text{I}_{0.48}$  alloy nanowires with regular square-shaped cross section has a single crystallinity nature.

Traditionally, semiconductor nanowires can be obtained by a CVD method through a vapor–liquid–solid (V–L–S) growth mechanism [9, 44, 45]. During the V–L–S growth process of the nanowires, metal nanoclusters are usually used as the catalysts. Besides, a self-assembled vapor-phase growth process without metal catalysts has also been demonstrated as an excellent approach to synthesize nanowires [12, 46, 47], which eliminates concern about metal contamination in the nanowire products. For the self-assembled vapor-phase growth process, the most important phenomenon is the selective crystal growth at the vapor–solid interface, which dictates the properties of obtained nanowires [43, 48]. During the CVD process, the growth is typically determined by the supply of vapor source, which is mainly controlled by the growth temperature and pressure [49–52]. Furthermore, when the  $\text{Si}/\text{SiO}_2$  substrate lacks constraint of specific lattice ordering in substrate surface, the perovskite nanowires grown on  $\text{Si}/\text{SiO}_2$  substrate tend to 3D vertical growth with somehow random orientations.

Figures 2(a) and 2(b) illustrate laser-induced halide ion phase segregation process in a typical perovskite  $\text{CsPbBr}_{2.52}\text{I}_{0.48}$  nanowire.

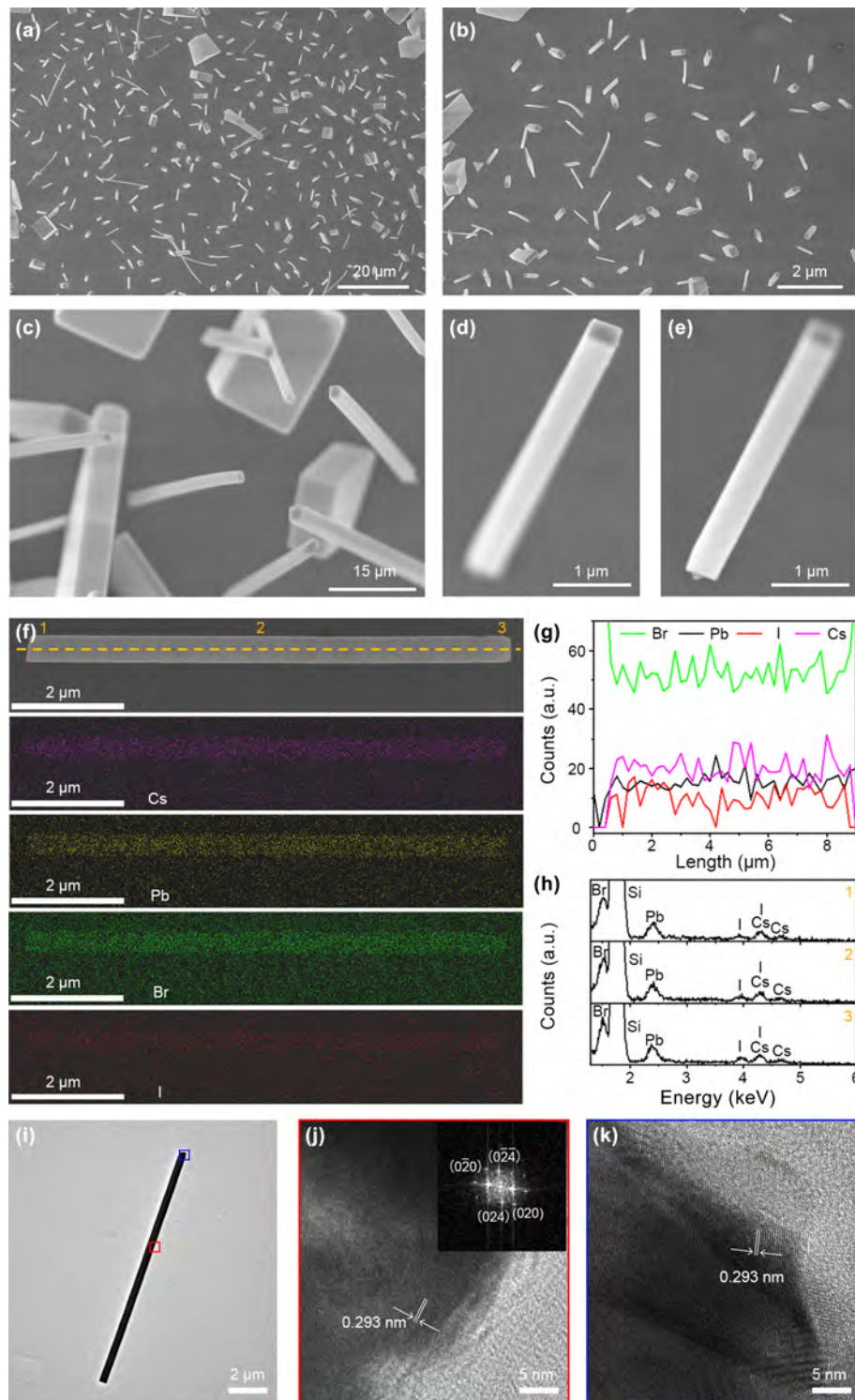


**Figure 1** Structural characterizations of the  $\text{CsPbBr}_{2.52}\text{I}_{0.48}$  perovskite alloy nanowires. (a) and (b) Low-resolution SEM images of the  $\text{CsPbBr}_{2.52}\text{I}_{0.48}$  nanowires on the Si/SiO<sub>2</sub> substrate. (c)–(e) SEM images of some typical single nanowires. (f) 2D EDX elements mapping of a single  $\text{CsPbBr}_{2.52}\text{I}_{0.48}$  nanowire before a focused 375 nm laser illumination. (g) Elemental composition analysis along a single nanowire, as indicated in orange dotted line in (f). (h) EDX spectra from three typical positions (1)–(3) along the length direction of the wire as indicated in (f). (i) Low-resolution TEM image of a selected nanowire. (j) and (k) HR-TEM images of two typical positions on the nanowire (red and blue squares as indicated in (i)). Inset: the corresponding FFT pattern from TEM image.

This phase separation process is thought to be related to differences in photochemical stability of different halogens in perovskite nanowires. Under continuous laser illumination, photogenerated carriers would sample a significant volume fraction of the lattice before radiatively recombining. During diffusion, carriers have

ample opportunity to survey multiple crystallographic domains and should rapidly thermalize and become trapped upon encountering any I-rich low-band-gap region (Fig. 2(b)). The change in band structure between an I-rich domain and the uniformly mixed perovskite could also generate an electric field that might further aid



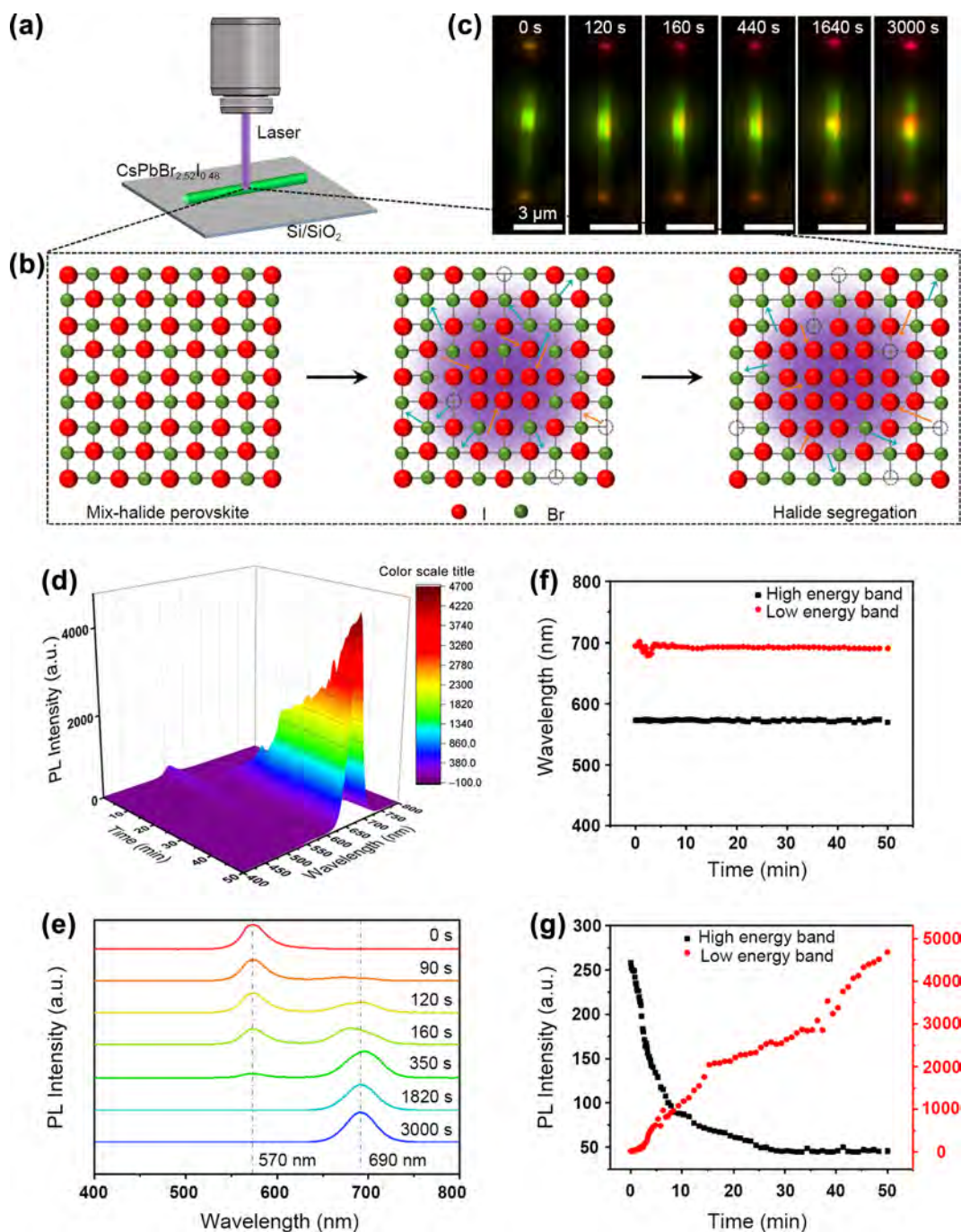


**Figure 2** Optical characterization of a single CsPbBr<sub>2.52</sub>I<sub>0.48</sub> nanowire due to phase segregation under a focused 375 nm laser illumination. (a) and (b) Schematic of the laser-induced halide ion phase segregation process in a typical CsPbBr<sub>2.52</sub>I<sub>0.48</sub> nanowire. (c) Dark-field emission images of a typical nanowire under a focused 375 nm laser illumination at 0, 120, 160, 440, 1640 and 3000 s, respectively. Scale bar is 3 μm. (d) 3D-PL spectra with peak centered at 570 and 690 nm continuously recorded from 0–50 min. (e) PL spectra of a nanowire under the 375 nm laser illumination at 0, 90, 120, 160, 350, 1820 and 3000 s, respectively. (f) Time-dependent emissions and (g) PL intensity at high (570 nm) and low energy band (690 nm) from  $t = 0$  to 50 min, respectively.

in sweeping carriers into the I-rich domain. Thus, nearly all of the PL should come from the radiative relaxation of carriers trapped in I-rich regions [53].

The optical measurements of a single perovskite CsPbBr<sub>2.52</sub>I<sub>0.48</sub> nanowire are shown in Figs. 2(c)–2(g). The evolution of dark-field real-color images of a single CsPbBr<sub>2.52</sub>I<sub>0.48</sub> nanowire under a focused 375 nm laser ( $P = 9.7 \times 10^2$  W/cm<sup>2</sup>) are shown in Fig. 2(c), using a confocal microscopy system (Fig. S4 in the ESM). As can be seen, the center of the nanowires is illuminated by the laser from

green emission to red emission as the excitation time increases (0–3000 s), which indicates the laser-induced phase segregation in light region. Figures 2(d) and 2(e) show the change in PL spectra of a single CsPbBr<sub>2.52</sub>I<sub>0.48</sub> nanowire under a 375 nm laser illumination from 0 to 50 min. Figure 2(d) depicts the 3D PL spectra variation of high- and low-energy band emissions, while the spectra of typical irradiation times (0, 90, 120, 160, 350, 1820 and 3000 s) selected for typical irradiation times are shown in Fig. 2(e). Upon photoexcitation, a PL emission peak at 570 nm appear immediately

(0 s), which is ascribed to the band-to-band emission of CsPbBr<sub>2.52</sub>I<sub>0.48</sub> alloy nanowires [54]. With the further increased illumination time, the PL intensity at 690 nm is risen continuously accompanied with the gradual dropped of counterpart emission peak at 570 nm. It is worth noting that the full width at half maximum (FWHM) of emission peak at 690 nm is ~ 60 nm (120 and 160 s), which originates from those CsPbBr<sub>2.52</sub>I<sub>0.48</sub> nanowires located at the edge of the laser spot without receiving enough power density to trigger phase segregation [24, 55]. After that, the PL emission peak at 690 nm occupy a completely dominant role with negligible PL emission peak at 570 nm under the laser illumination time of 3000 s. During this laser excited process (0–3000 s), the intensity difference of the PL spectra further suggests the halide phase segregation occurs at the excited positions. Furthermore, Fig. S5 in the ESM shows the dark-field emission images of wafer-scale nanowires under the unfocused 405 nm laser exciting from  $t = 0$  to 50 min. As can be seen, the emission color of these nanowires varies from orange to red further indicating the occurrence of phase segregation of CsPbBr<sub>2.52</sub>I<sub>0.48</sub> nanowires. The time-dependent PL spectra indicate a dual-wavelength emission at 570 and 690 nm as a consequence of halide ion segregation, where no obvious peak shift

at phase segregation process (as indicated in Fig. 2(f)). Meanwhile, the PL emission intensity of the high energy band (HEB) is falling continuously, while the intensity of low energy band (LEB) continues to rise (Fig. 2(g)) accordingly. The PL emission peaks changes of CsPbBr<sub>2.52</sub>I<sub>0.48</sub> nanowires demonstrate the existence of phase segregation, owing to the laser-induced halide ion migration [35]. In addition, element distribution of the perovskite nanowires show no obvious changes before (Figs. 1(h)–1(j)) and after (Fig. S6 in the ESM) the 375 nm laser illumination, which may be attributed to that the excessive Br<sup>-</sup> ions tend to substitute the I<sup>-</sup> ions in the perovskite lattice, as Pb<sup>2+</sup>/Br<sup>-</sup> binding is more favorable in mixed halide perovskite binding formation when stopping the laser illumination to EDX elemental analysis [56–58]. Furthermore, laser-induced halide ion phase segregation process based on different composition perovskite CsPbBr<sub>x</sub>I<sub>3-x</sub> ( $x = 2.56, 1.86, 1.38$  and  $1.17$ ) nanowires is shown in Figs. S7–S10 in the ESM.

In order to investigate the emission changes of these perovskite nanowires under a laser excitation with about 600 s intervals, the time-dependent PL spectra and corresponding dark-field images are recorded in Fig. 3, respectively. Figure 3(a) exhibits twelve real-color images of a typical CsPbBr<sub>2.52</sub>I<sub>0.48</sub> nanowire under a 375 nm

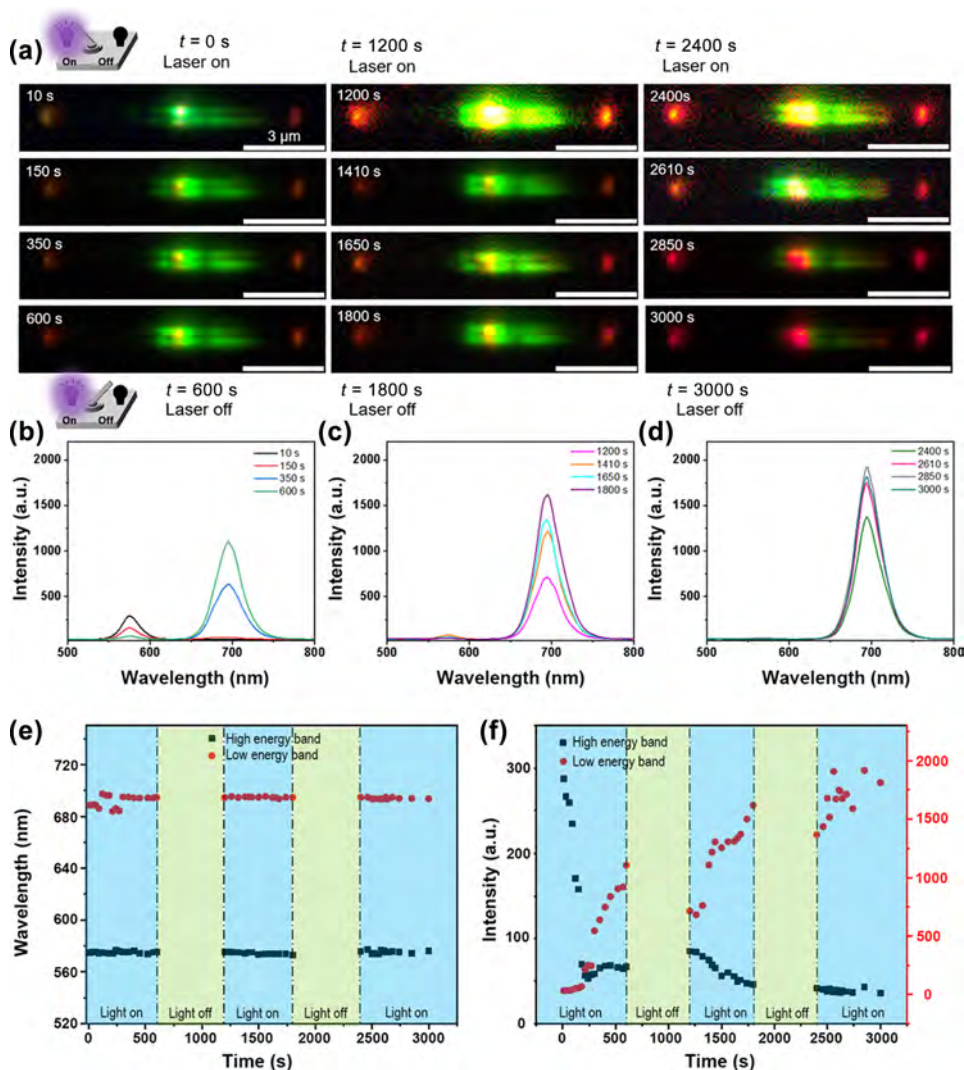


**Figure 3** Dual-wavelength emission of a perovskite alloy nanowire. (a) Dark-field images and (b)–(d) corresponding spectra of nanowires with three switch cycles under a focused 375 nm laser illumination. Scale bar is 3  $\mu\text{m}$ . (e) Time-dependent PL emissions and (f) PL intensity at high- (570 nm) and low-energy band (690 nm), respectively.



laser illumination at different exciting time from 0–3000 s. The corresponding PL spectra are shown in Figs. 3(b)–3(d), which shows agreement with the spectral variation trend under a continuous laser illumination in Fig. 2. When the laser is turned on (at the time of 0 s), the PL emission intensity of low energy band (690 nm) is gradually increased, while the high energy band emission (570 nm) is decreased accordingly and the dark-field emission images ( $t = 10, 150, 350$  and  $600$  s) and corresponding PL spectra (Fig. 3(b)) are recorded. Then the laser is turned off (at the time of 600 s) and on (at the time of 1200 s) again for the second cycle. Under laser illumination, dark-field emission images ( $t = 1200, 1410, 1650$  and  $1800$  s) and corresponding spectra (Fig. 3(c)) are also recorded respectively, which indicate the PL peak at 690 nm plays a dominant role. Then the laser is turned off at  $t = 1800$  s and turned on again at  $t = 2400$  s. On the third switching cycle, the dark-field emission images of four exciting time ( $t = 2400, 2610, 2850$  and  $3000$  s) are shown in Figs. 3(a) and 3(d). And the PL emission intensity of low energy band (690 nm) continues to increase and approaches saturation (Fig. 3(d)). Figure 3(e) shows the time-dependent PL emissions of the nanowires, which indicates that the PL peak has no significant shift during the periodic turned on/off laser. Figure 3(f) shows the time-dependent PL intensity of both emissions at 570 and 690 nm respectively, in which the PL emission intensity of the high energy band tends to increase with the decrease of low energy band. It is noted that the phase segregation stops when the laser is turned off and the PL emission intensity of low energy band has a backtracking when laser is turned on again as shown in Fig. 3(f). The phase segregation of nanowire cannot completely return to the mixed phase, which may be caused by the uniform strains produced from the laser illumination-induced temperature variation and the uniform strains can be easily relaxed through the global volume changes [26].

One-dimensional (1D) nanowires with good waveguiding and oscillating cavity offer a robust material platform for complex nanophotonics and functional optoelectronic devices [59–61]. With the phase segregation of perovskite alloy components under laser illumination, optical switch is constructed, as shown in Fig. 4, by defining the output intensity ratio of  $I_{O-LEB}$  to  $I_{O-HEB}$ . Figure 4(a) shows the energy band structures of the perovskite  $\text{CsPbBr}_{2.52}\text{I}_{0.48}$  nanowires resulted from laser-induced phase segregation. When a typical nanowire is excited by a 375 nm focused laser, the output waveguide signal is changed with the phase separation at the excitation positions, as shown in Figs. 4(b)(i)–4(b)(iii). At the beginning, an active waveguide occurs along the wire through re-absorption and re-emission processes for the high energy band emission (570 nm) as exhibited in Fig. 4(b)(i). Then, with the emergence of phase segregation, the PL emission (690 nm) of the low energy band is expected to be passively guided along the axial of wire through total internal reflections, as shown in Figs. 4(b)(ii) and 4(b)(iii), respectively. It can be seen that the  $I_{O-LEB}$  is increased with the decrease of  $I_{O-HEB}$  (Figs. 4(c)–4(e)), which means that the ratio of  $I_{O-LEB}/I_{O-HEB}$  is increased. Here, the optical switch of 0 and 1 is defined by  $I_{O-LEB}/I_{O-HEB} < 1$  and  $I_{O-LEB}/I_{O-HEB} \geq 1$ , as shown in Fig. 4(f), which corresponding to the blue and yellow regions, respectively (Fig. 4(g)). Thus, according to the results, an time-delay optical switch is successfully realized based on these perovskite nanowires controlled by a laser beam.

#### 4 Conclusions

In summary, the self-assembled perovskite  $\text{CsPbBr}_{2.52}\text{I}_{0.48}$  alloy nanowires were successfully prepared via a two-step CVD method. Structural analysis reveals that the wires have high-quality single crystalline with square shaped cross sections. Optical

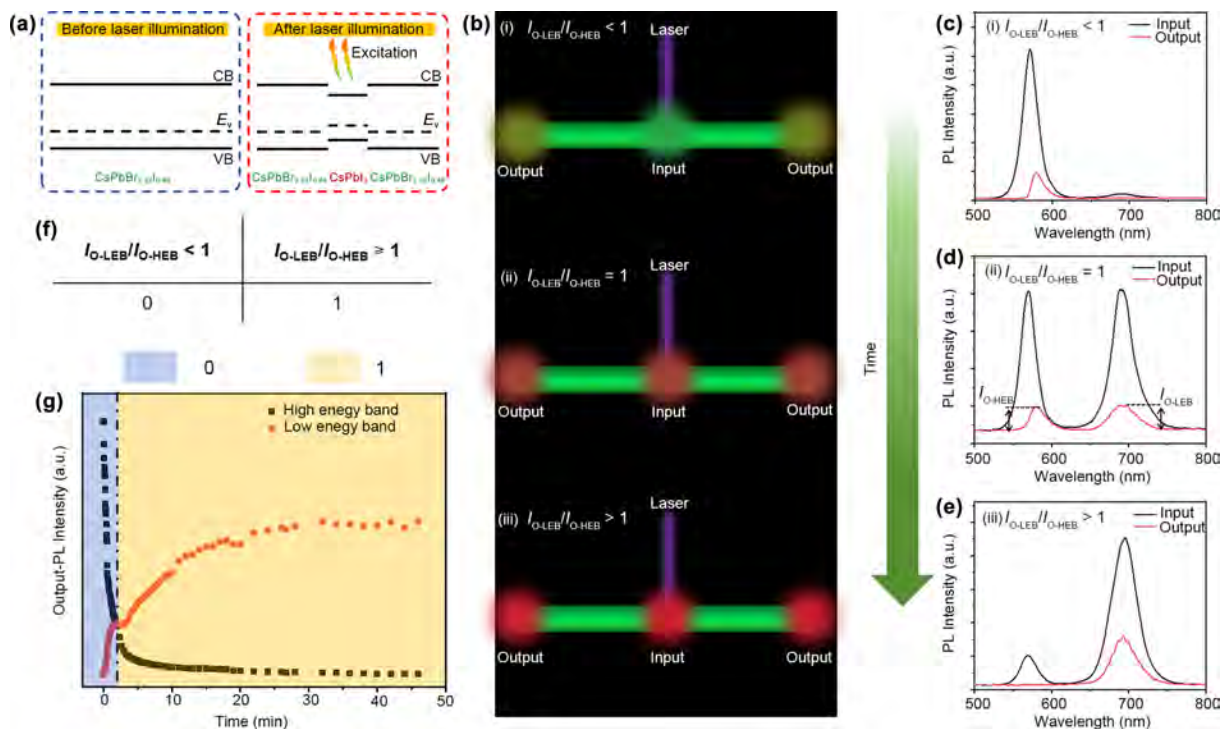


**Figure 4** Optical switch based on the  $\text{CsPbBr}_{2.52}\text{I}_{0.48}$  perovskite nanowires under a focused laser illumination. (a) Schematic bandgap diagram of the perovskite nanowire before and after the laser illumination. (b) Schematic diagram of signal variation (i)–(iii) at the output end of a single nanowire with the increase of laser excitation time. (c)–(e) Corresponding PL spectra from the ends of the wires. (f) The optical logic information code of optical switch. (g) Output PL intensity of high and low energy band emission and logic information.

characterization indicates dual-wavelength emission peaks at 570 and 690 nm as a consequence of halide ion segregation under a focused laser illumination. Additionally, time-dependent PL spectra show a completely different PL emissions for low energy band (690 nm) and high energy band (570 nm). These unique results suggesting a phase segregation occurs at the nanowires under a 375 nm laser illumination. Moreover, an optical switch based on the CsPbBr<sub>2.52</sub>I<sub>0.48</sub> alloy nanowires are realized controlled by a laser beam. These phase segregation of perovskite alloy nanowires and laser induced optical switch may provide an excited opportunity for all-optical switching devices.

**Electronic Supplementary Material:** Supplementary material (CVD setup, SEM image, EDX spectra and optical photographs of the perovskite alloy nanowires, schematic diagram of confocal microscopy system and optoelectronic characterization of scale typical perovskite alloy nanowire under continue laser illumination) is available in the online version of this article at <https://doi.org/10.26599/NR.2025.94907119>.

### Data availability

All data needed to support the conclusions in the paper are presented in the manuscript and the Electronic Supplementary Material. Additional data related to this paper may be requested from the corresponding author upon request.

### Acknowledgements

The authors acknowledge the assistance of Instrumental Analysis Center Taiyuan University of Technology. The authors are grateful to the National Natural Science Foundation of China (No. 52373246), the Fundamental Research Program of Shanxi Provinces (No. 20210302123128) and the National Key Research and Development Program of China (No. 2022YFA1404201) for financial support.

### Declaration of competing interest

All the contributing authors report no conflict of interests in this work.

### Author contribution statement

P. F. G. and L. T. X. conceived and designed the research. Q. H. L. and X. Y. L. synthesized the perovskite alloy nanowires. Q. H. L., X. Y. L. and Z. H. S. performed optical characterization. Q. H. L., P. F. G. and X. S. wrote the related discussions. All authors discussed the results and commented on the manuscript.

### Use of AI statement

None.

### References

- Zhang, Z. J.; Suchan, K.; Li, J.; Hetherington, C.; Kiligaris, A.; Unger, E.; Scheblykin, I. G.; Wallentin, J. Vertically aligned CsPbBr<sub>3</sub> nanowire arrays with template-induced crystal phase transition and stability. *J. Phys. Chem. C* **2021**, *125*, 4860–4868.
- Gao, Y.; Zhao, L. Y.; Shang, Q. Y.; Zhong, Y. G.; Liu, Z.; Chen, J.; Zhang, Z. P.; Shi, J.; Du, W. N.; Zhang, Y. F. et al. Ultrathin CsPbX<sub>3</sub> nanowire arrays with strong emission anisotropy. *Adv. Mater.* **2018**, *30*, 1801805.
- Li, J.; Xu, J.; Bao, Y. N.; Li, J. L.; Wang, H. S.; He, C. Y.; An, M. Q.; Tang, H. Y.; Sun, Z. G.; Fang, Y. R. et al. Anion-exchange driven phase transition in cspbi<sub>3</sub> nanowires for fabricating epitaxial perovskite heterojunctions. *Adv. Mater.* **2022**, *34*, 2109867.
- Zhang, X. H.; Wang, C. Y.; Sun, Q. S.; Wu, J. X.; Dai, Y.; Li, E. L.; Wu, J. S.; Chen, H. P.; Duan, S. M.; Hu, W. P. Inorganic halide perovskite nanowires/conjugated polymer heterojunction-based optoelectronic synaptic transistors for dynamic machine vision. *Nano Lett.* **2024**, *24*, 4132–4140.
- Zhang, Z. J.; Lamers, N.; Sun, C.; Hetherington, C.; Scheblykin, I. G.; Wallentin, J. Free-standing metal halide perovskite nanowire arrays with blue-green heterostructures. *Nano Lett.* **2022**, *22*, 2941–2947.
- Meng, Y.; Lan, C. Y.; Li, F. Z.; Yip, S.; Wei, R. J.; Kang, X. L.; Bu, X. M.; Dong, R. T.; Zhang, H.; Ho, J. C. Direct vapor–liquid–solid synthesis of all-inorganic perovskite nanowires for high-performance electronics and optoelectronics. *ACS Nano* **2019**, *13*, 6060–6070.
- Dou, L. T.; Lai, M. L.; Kley, C. S.; Yang, Y. M.; Bischak, C. G.; Zhang, D. D.; Eaton, S. W.; Ginsberg, N. S.; Yang, P. D. Spatially resolved multicolor CsPbX<sub>3</sub> nanowire heterojunctions via anion exchange. *Proc. Natl. Acad. Sci. USA* **2017**, *114*, 7216–7221.
- Liu, P.; He, X. X.; Ren, J. H.; Liao, Q.; Yao, J. N.; Fu, H. B. Organic–inorganic hybrid perovskite nanowire laser arrays. *ACS Nano* **2017**, *11*, 5766–5773.
- Meng, Y.; Zhang, Y. X.; Lai, Z. X.; Wang, W.; Wang, W. J.; Li, Y. Z.; Li, D. J.; Xie, P. S.; Yin, D.; Chen, D. et al. Au-seeded CsPbI<sub>3</sub> nanowire optoelectronics via exothermic nucleation. *Nano Lett.* **2023**, *23*, 812–819.
- Song, J. P.; Shang, Q. Y.; Deng, X. Y.; Liang, Y.; Li, C.; Liu, X. F.; Xiong, Q. H.; Zhang, Q. Continuous-wave pumped perovskite lasers with device area below 1 μm<sup>2</sup>. *Adv. Mater.* **2023**, *35*, 2302170.
- Gao, Y.; Li, X. H.; Liu, W. W.; Xing, X. Y.; Long, H.; Wang, K.; Wang, B.; Lu, P. X. Highly tunable enhancement and switching of nonlinear emission from all-inorganic lead halide perovskites via electric field. *Nano Lett.* **2021**, *21*, 10230–10237.
- Tang, B.; Hu, Y. J.; Lu, J.; Dong, H. X.; Mou, N. L.; Gao, X. Y.; Wang, H.; Jiang, X. W.; Zhang, L. Energy transfer and wavelength tunable lasing of single perovskite alloy nanowire. *Nano Energy* **2020**, *71*, 104641.
- Mali, S. S.; Patil, J. V.; Shao, J. Y.; Zhong, Y. W.; Rondiya, S. R.; Dzade, N. Y.; Hong, C. K. Phase-heterojunction all-inorganic perovskite solar cells surpassing 21.5% efficiency. *Nat. Energy* **2023**, *8*, 989–1001.
- Li, X.; Liu, C.; Ding, F.; Lu, Z. Y.; Gao, P.; Huang, Z. W.; Dang, W. Q.; Zhang, L. Q.; Lin, X. H.; Ding, S. M. et al. Ultra-stable and sensitive ultraviolet photodetectors based on monocrystalline perovskite thin films. *Adv. Funct. Mater.* **2023**, *33*, 2213360.
- Cao, Y. B.; Zhang, D. Q.; Zhang, Q. P.; Qiu, X.; Zhou, Y.; Poddar, S.; Fu, Y.; Zhu, Y. D.; Liao, J. F.; Shu, L. et al. High-efficiency, flexible and large-area red/green/blue all-inorganic metal halide perovskite quantum wires-based light-emitting diodes. *Nat. Commun.* **2023**, *14*, 4611.
- Otero-Martínez, C.; Ye, J. Z.; Sung, J.; Pastoriza-Santos, I.; Pérez-Juste, J.; Xia, Z. G.; Rao, A.; Hoye, R. L. Z.; Polavarapu, L. Colloidal metal-halide perovskite nanoplatelets: Thickness-controlled synthesis, properties, and application in light-emitting diodes. *Adv. Mater.* **2022**, *34*, 2107105.
- Fan, C.; Xu, X.; Yang, K.; Jiang, F.; Wang, S. Y.; Zhang, Q. L. Controllable epitaxial growth of core–shell PbSe@CsPbBr<sub>3</sub> wire heterostructures. *Adv. Mater.* **2018**, *30*, 1804707.
- Bao, C. X.; Yang, J.; Bai, S.; Xu, W. D.; Yan, Z. B.; Xu, Q. Y.; Liu, J. M.; Zhang, W. J.; Gao, F. High performance and stable all-inorganic metal halide perovskite-based photodetectors for optical

- communication applications. *Adv. Mater.* **2018**, *30*, 1803422.
- [19] Feng, L. K.; Wang, Z. M.; Wang, W. H.; Li, F.; Ren, Y. J.; Wang, Y. Constructing Urbach-tail-free and low-threshold perovskite heteronanowire lasers toward all-optical switching. *ACS Photonics* **2022**, *9*, 459–465.
- [20] Du, W. N.; Wu, X. X.; Zhang, S.; Sui, X. Y.; Jiang, C. X.; Zhu, Z. Y.; Shang, Q. Y.; Shi, J. W.; Yue, S.; Zhang, Q. et al. All optical switching through anisotropic gain of CsPbBr<sub>3</sub> single crystal microplatelet. *Nano Lett.* **2022**, *22*, 4049–4057.
- [21] Steele, J. A.; Lai, M. L.; Zhang, Y.; Lin, Z. N.; Hofkens, J.; Roeffaers, M. B. J.; Yang, P. D. Phase transitions and anion exchange in all-inorganic halide perovskites. *Acc. Mater. Res.* **2020**, *1*, 3–15.
- [22] Xue, J.; Yang, D. D.; Cai, B.; Xu, X. B.; Wang, J.; Ma, H.; Yu, X. C.; Yuan, G. L.; Zou, Y. S.; Song, J. Z. et al. Photon-induced reversible phase transition in CsPbBr<sub>3</sub> perovskite. *Adv. Funct. Mater.* **2019**, *29*, 1807922.
- [23] Mao, W. X.; Hall, C. R.; Bernardi, S.; Cheng, Y. B.; Widmer-Cooper, A.; Smith, T. A.; Bach, U. Light-induced reversal of ion segregation in mixed-halide perovskites. *Nat. Mater.* **2021**, *20*, 55–61.
- [24] Draguta, S.; Sharia, O.; Yoon, S. J.; Brennan, M. C.; Morozov, Y. V.; Manser, J. S.; Kamat, P. V.; Schneider, W. F.; Kuno, M. Rationalizing the light-induced phase separation of mixed halide organic–inorganic perovskites. *Nat. Commun.* **2017**, *8*, 200.
- [25] Stoumpos, C. C.; Kanatzidis, M. G. The renaissance of halide perovskites and their evolution as emerging semiconductors. *Acc. Chem. Res.* **2015**, *48*, 2791–2802.
- [26] Bischak, C. G.; Hetherington, C. L.; Wu, H.; Aloni, S.; Ogletree, D. F.; Limmer, D. T.; Ginsberg, N. S. Origin of reversible photoinduced phase separation in hybrid perovskites. *Nano Lett.* **2017**, *17*, 1028–1033.
- [27] Suchan, K.; Merdasa, A.; Rehmann, C.; Unger, E. L.; Scheblykin, I. G. Complex evolution of photoluminescence during phase segregation of MAPb(I<sub>1-x</sub>Br<sub>x</sub>)<sub>3</sub> mixed halide perovskite. *J. Lumin.* **2020**, *221*, 117073.
- [28] Galisteo-López, J. F.; Anaya, M.; Calvo, M. E.; Míguez, H. Environmental effects on the photophysics of organic–inorganic halide perovskites. *J. Phys. Chem. Lett.* **2015**, *6*, 2200–2205.
- [29] Li, W.; Rothmann, M. U.; Liu, A.; Wang, Z. Y.; Zhang, Y. P.; Pascoe, A. R.; Lu, J. F.; Jiang, L. C.; Chen, Y.; Huang, F. Z. et al. Phase segregation enhanced ion movement in efficient inorganic CsPbI<sub>2</sub>Br<sub>2</sub> solar cells. *Adv. Energy Mater.* **2017**, *7*, 1700946.
- [30] Gualdrón-Reyes, A. F.; Yoon, S. J.; Barea, E. M.; Agouram, S.; Muñoz-Sanjosé, V.; Meléndez, Á. M.; Niño-Gómez, M. E.; Mora-Seró, I. Controlling the phase segregation in mixed halide perovskites through nanocrystal size. *ACS Energy Lett.* **2019**, *4*, 54–62.
- [31] Wang, X.; Ling, Y. C.; Lian, X. J.; Xin, Y.; Dhungana, K. B.; Perez-Orive, F.; Knox, J.; Chen, Z. Z.; Zhou, Y.; Beery, D. et al. Suppressed phase separation of mixed-halide perovskites confined in endotaxial matrices. *Nat. Commun.* **2019**, *10*, 695.
- [32] Lin, C. K.; Zhang, Y.; Gao, M. Y.; Lin, J. A.; Le, H. K. D.; Lin, Z. N.; Yang, P. D. Controlling the phase transition in CsPbI<sub>3</sub> nanowires. *Nano Lett.* **2022**, *22*, 2437–2443.
- [33] Kong, Q.; Lee, W.; Lai, M. L.; Bischak, C. G.; Gao, G. P.; Wong, A. B.; Lei, T.; Yu, Y.; Wang, L. W.; Ginsberg, N. S. et al. Phase-transition-induced p-n junction in single halide perovskite nanowire. *Proc. Natl. Acad. Sci. USA* **2018**, *115*, 8889–8894.
- [34] Feng, S. N.; Ju, Y.; Duan, R. T.; Man, Z. Q.; Li, S. Y.; Hu, F. R.; Zhang, C. F.; Tao, S. X.; Zhang, W. H.; Xiao, M. et al. Complete suppression of phase segregation in mixed-halide perovskite nanocrystals under periodic heating. *Adv. Mater.* **2024**, *36*, 2308032.
- [35] Zhang, H. C.; Fu, X.; Tang, Y.; Wang, H.; Zhang, C. F.; Yu, W. W.; Wang, X. Y.; Zhang, Y.; Xiao, M. Phase segregation due to ion migration in all-inorganic mixed-halide perovskite nanocrystals. *Nat. Commun.* **2019**, *10*, 1088.
- [36] Brennan, M. C.; Toso, S.; Pavlovets, I. M.; Zhukovskiy, M.; Marras, S.; Kuno, M.; Manna, L.; Baranov, D. Superlattices are greener on the other side: How light transforms self-assembled mixed halide perovskite nanocrystals. *ACS Energy Lett.* **2020**, *5*, 1465–1473.
- [37] Tang, X. F.; van den Berg, M.; Gu, E. N.; Horneber, A.; Matt, G. J.; Osvet, A.; Meixner, A. J.; Zhang, D.; Brabec, C. J. Local observation of phase segregation in mixed-halide perovskite. *Nano Lett.* **2018**, *18*, 2172–2178.
- [38] Yoon, S. J.; Draguta, S.; Manser, J. S.; Sharia, O.; Schneider, W. F.; Kuno, M.; Kamat, P. V. Tracking iodide and bromide ion segregation in mixed halide lead perovskites during photoirradiation. *ACS Energy Lett.* **2016**, *1*, 290–296.
- [39] Hoke, E. T.; Slotcavage, D. J.; Dohner, E. R.; Bowring, A. R.; Karunadasa, H. I.; McGehee, M. D. Reversible photo-induced trap formation in mixed-halide hybrid perovskites for photovoltaics. *Chem. Sci.* **2015**, *6*, 613–617.
- [40] Eperon, G. E.; Hörantner, M. T.; Snaith, H. J. Metal halide perovskite tandem and multiple-junction photovoltaics. *Nat. Rev. Chem.* **2017**, *1*, 0095.
- [41] Leijtens, T.; Bush, K. A.; Prasanna, R.; McGehee, M. D. Opportunities and challenges for tandem solar cells using metal halide perovskite semiconductors. *Nat. Energy* **2018**, *3*, 828–838.
- [42] Balakrishna, R. G.; Kobosko, S. M.; Kamat, P. V. Mixed halide perovskite solar cells. consequence of iodide treatment on phase segregation recovery. *ACS Energy Lett.* **2018**, *3*, 2267–2272.
- [43] Samiei, S.; Soheily, E.; Vighnesh, K.; Nabyouni, G.; Rogach, A. L. Exploring CsPbX<sub>3</sub> (X = Cl, Br, I) perovskite nanocrystals in amorphous oxide glasses: Innovations in fabrication and applications. *Small* **2024**, *20*, 2307972.
- [44] Meyers, J. K.; Kim, S.; Hill, D. J.; Cating, E. E. M.; Williams, L. J.; Kumbhar, A. S.; McBride, J. R.; Papanikolas, J. M.; Cahoon, J. F. Self-catalyzed vapor–liquid–solid growth of lead halide nanowires and conversion to hybrid perovskites. *Nano Lett.* **2017**, *17*, 7561–7568.
- [45] Guo, P. F.; Liu, D.; Shen, X.; Lv, Q. H.; Wu, Y.; Yang, Q.; Li, P.; Hao, Y. Y.; Ho, J. C.; Yu, K. M. On-wire axial perovskite heterostructures for monolithic dual-wavelength laser. *Nano Energy* **2022**, *92*, 106778.
- [46] Chen, J.; Fu, Y. P.; Samad, L.; Dang, L. N.; Zhao, Y. Z.; Shen, S. H.; Guo, L. J.; Jin, S. Vapor-phase epitaxial growth of aligned nanowire networks of cesium lead halide perovskites (CsPbX<sub>3</sub>, X = Cl, Br, I). *Nano Lett.* **2017**, *17*, 460–466.
- [47] Wang, Y. P.; Sun, X.; Shivanna, R.; Yang, Y. B.; Chen, Z. Z.; Guo, Y. W.; Wang, G. C.; Wertz, E.; Deschler, F.; Cai, Z. H. et al. Photon transport in one-dimensional incommensurately epitaxial CsPbX<sub>3</sub> arrays. *Nano Lett.* **2016**, *16*, 7974–7981.
- [48] Shoaib, M.; Zhang, X. H.; Wang, X. X.; Zhou, H.; Xu, T.; Wang, X.; Hu, X. L.; Liu, H. W.; Fan, X. P.; Zheng, W. H. et al. Directional growth of ultralong CsPbBr<sub>3</sub> perovskite nanowires for high-performance photodetectors. *J. Am. Chem. Soc.* **2017**, *139*, 15592–15595.
- [49] Zhu, Z. T.; Suzuki, M.; Nagashima, K.; Yoshida, H.; Kanai, M.; Meng, G.; Anzai, H.; Zhuge, F. W.; He, Y.; Boudot, M. et al. Rational concept for reducing growth temperature in vapor–liquid–solid process of metal oxide nanowires. *Nano Lett.* **2016**, *16*, 7495–7502.
- [50] Zhang, L. Q.; Wang, Y. L.; Chu, A. S.; Zhang, Z. W.; Liu, M. M.; Shen, X. H.; Li, B. L.; Li, X.; Yi, C.; Song, R. et al. Facet-selective growth of halide perovskite/2D semiconductor van der Waals heterostructures for improved optical gain and lasing. *Nat. Commun.* **2024**, *15*, 5484.
- [51] Huangfu, Y.; Qin, B.; Lu, P.; Zhang, Q. K.; Li, W.; Liang, J. Y.; Liang, Z. M.; Liu, J. L.; Liu, M. M.; Lin, X. H. et al. Low temperature synthesis of 2D p-type  $\alpha$ -In<sub>2</sub>Te<sub>3</sub> with fast and broadband photodetection. *Small* **2024**, *20*, 2309620.
- [52] Liu, X.; Sun, G. Z.; Chen, P.; Liu, J. C.; Zhang, Z. W.; Li, J.; Ma, H. F.; Zhao, B.; Wu, R. X.; Dang, W. Q. et al. High-performance asymmetric electrodes photodiode based on Sb/WSe<sub>2</sub> heterostructure. *Nano Res.* **2019**, *12*, 339–344.
- [53] Slotcavage, D. J.; Karunadasa, H. I.; McGehee, M. D. Light-induced



- phase segregation in halide-perovskite absorbers. *ACS Energy Lett.* **2016**, *1*, 1199–1205.
- [54] Zhang, Y.; Lu, D.; Gao, M. Y.; Lai, M. L.; Lin, J.; Lei, T.; Lin, Z. Z.; Quan, L. N.; Yang, P. D. Quantitative imaging of anion exchange kinetics in halide perovskites. *Proc. Natl. Acad. Sci. USA* **2019**, *116*, 12648–12653.
- [55] Muscarella, L. A.; Hutter, E. M.; Wittmann, F.; Woo, Y. W.; Jung, Y. K.; McGovern, L.; Versluis, J.; Walsh, A.; Bakker, H. J.; Ehrler, B. Lattice compression increases the activation barrier for phase segregation in mixed-halide perovskites. *ACS Energy Lett.* **2020**, *5*, 3152–3158.
- [56] Yoon, S. J.; Kuno, M.; Kamat, P. V. *Shift happens*. how halide ion defects influence photoinduced segregation in mixed halide perovskites. *ACS Energy Lett.* **2017**, *2*, 1507–1514.
- [57] Chen, W. J.; Mao, W. X.; Bach, U.; Jia, B.; Wen, X. M. Tracking dynamic phase segregation in mixed-halide perovskite single crystals under two-photon scanning laser illumination. *Small Methods* **2019**, *3*, 1900273.
- [58] Shynkarenko, Y.; Bodnarchuk, M. I.; Bernasconi, C.; Berezovska, Y.; Verteletskyi, V.; Ochsenbein, S. T.; Kovalenko, M. V. Direct synthesis of quaternary alkylammonium-capped perovskite nanocrystals for efficient blue and green light-emitting diodes. *ACS Energy Lett.* **2019**, *4*, 2703–2711.
- [59] Xiong, Y. T.; Xu, X. Z.; Chen, B.; Xu, X. B. Highly crystalized MAPbX<sub>3</sub> perovskite triangular nanowire arrays for optoelectronic applications. *Adv. Mater.* **2024**, *36*, 2310427.
- [60] Li, D. J.; Meng, Y.; Zhang, Y. X.; Xie, P. S.; Zeng, Z. X.; Wang, W.; Lai, Z. X.; Wang, W. J.; Tsang, S. W.; Wang, F. et al. Selective surface engineering of perovskite microwire arrays. *Adv. Funct. Mater.* **2023**, *33*, 2302866.
- [61] Fan, C.; Zhu, M. Y.; Xu, X.; Wang, P.; Zhang, Q. L.; Dai, X. L.; Yang, K.; He, H. P.; Ye, Z. Z. Self-competitive growth of CsPbBr<sub>3</sub> planar nanowire array. *Nano Lett.* **2024**, *24*, 3750–3758.